# Impacts of Triple La Niña Events on Forest Gross Primary Productivity in China from 2020 to 2022

Wensi Ma<sup>1</sup>, Qiaoli Wu<sup>1\*</sup>, Wei He<sup>2,3</sup>, Jie Jiang<sup>1</sup>

Keywords: La Niña, Extreme Weather Events, Gross Primary Productivity, Remote Sensing Monitoring, Chinese Forests.

#### **Abstract**

Based on GOSIF GPP data and climate data, this study systematically explored the impact mechanism of triple La Niña event on gross primary productivity (GPP) of forest ecosystem in China from 2020 to 2022 and its physiological and ecological driving process. The results show that GPP in China forest presents a significant dynamic response of "initial inhibition-gradual recovery" to La Niña event. The annual average GPP decreased from 1799.27 Tg C year<sup>-1</sup> in the base period (2017-2018) to 1783.89 Tg C year<sup>-1</sup>, of which 2020 reached the lowest value of 1763.68 Tg C year<sup>-1</sup> in the study period, but showed strong recovery ability in the following two years, rising to 1804.54 Tg C year<sup>-1</sup>. Spatially, the subtropical monsoon region realized "V" recovery through vegetation adaptation, while the temperate monsoon region was inhibited by soil moisture at root zone and phenological delay. The temperate region showed "early stage determines late stage" characteristics, and the subtropical region formed "spring and autumn compensation" pattern. These differences are mainly due to the latitudinal difference regulation of La Niña event on East Asian monsoon system. The temperate region is adjusted by mid-high latitude circulation while the subtropical region directly responds to the continuous drought caused by tropical sea surface temperature (SST) anomaly. This study clarified the response of China forest to triple La Niña event through multiscale analysis, which provided important scientific basis for improving ecosystem model parameterization and predicting carbon sink function evolution.

#### 1. Introduction

Global warming and human activities have combined to alter the water cycle. Extreme climate events are becoming more frequent and unpredictable (Best and Darby, 2020). Terrestrial ecosystems have limited adaptive capacity and extreme climate events are likely to cause more severe, long-lasting, and irreversible damages to terrestrial ecosystems (Bastos et al., 2014).

In the three years from 2020 to 2022, the world ushered in the first triple La Niña events of this century, which had a significant impact on climate change in China. There is a close coupling relationship between the carbon cycle of terrestrial ecosystems and the water cycle, nutrient cycle and biodiversity of ecosystems. Therefore, under the strong influence of extreme climate events, the changes in the carbon cycle of terrestrial ecosystems will be a comprehensive manifestation of the response of terrestrial ecosystems to extreme climate events.

There is an urgent need for accurate assessment of forest carbon sink changes in China in the context of extreme climate change. This study intends to study the impact of extreme climate change on the gross primary productivity (GPP) of China's forest ecosystems by accounting for the triple La Niña events from 2020 to 2022. This study could provide a scientific basis for forestry management and help us better understand and predict the response of forest carbon sycle to future climate change scenarios(Wolf, 2023).

# 2. Study Area and Datas

#### 2.1 Study Area

China forest ecosystem has significant global ecological importance. It is not only an important carbon sink area in the world, but also an ideal place to study vegetation-climate interaction. In recent years, vegetation carbon storage has been significantly improved through ecological projects such as returning farmland to forest. In terms of biodiversity, it covers a variety of climate zone types from tropical to cold temperate zone. Forest in China has important scientific value and practical significance as a research area.

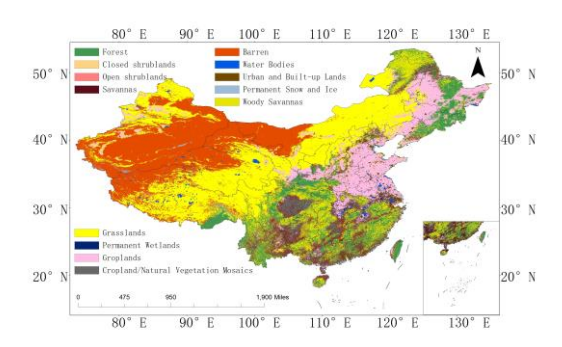


Figure 1. Regional Land Cover Types Map of China.

<sup>&</sup>lt;sup>1</sup> School of Geomatics and Urban Spatial Informatics, Beijing University of Civil Engineering and Architecture-Beijing, China - a13128463@163.com, wuqiaoli@bucea.edu.cn, jiangjie@bucea.edu.cn

<sup>&</sup>lt;sup>2</sup> Zhejiang Institute of Carbon Neutrality Innovation, Zhejiang University of Technology -Hangzhou, Zhejiang, China - wei.he@zjut.edu.cn

<sup>&</sup>lt;sup>3</sup> International Institute of Earth System Science, Nanjing University -Nanjing, Jiangsu, China

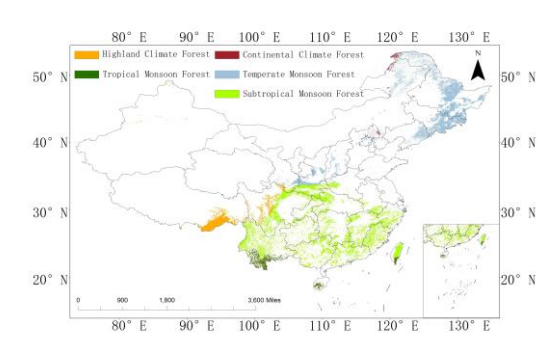


Figure 2. Forest cover in five climatic regions of China. Orange yellow is plateau mountain climate forest area. Reddish brown is temperate continental climate forest area. Dark green is tropical monsoon climate forest area. Light green is subtropical monsoon climate forest area. Sky blue is temperate monsoon climate forest area.

#### 2.2 GPP Data

This study used the GOSIF GPP (Global, OCO-2-based SIF-derived Gross Primary Productivity) dataset, a global total primary productivity estimation product based on sunlight induced chlorophyll fluorescence (SIF) and remote sensing data. The dataset is an OCO-2 based Global SIF product (GOSIF) developed by Sun Yat-sen University and a linear relationship between SIF and GPP, plotting global GPP for the period 2000 to 2024 at 0.05° spatial resolution and 8 day (and monthly) time steps.

Due to its high spatial and temporal resolution and direct correlation with photosynthesis, the dataset is widely used for vegetation productivity monitoring, ecosystem carbon cycling studies and climate change impact assessments.

GOSIF GPP can effectively capture GPP dynamics at regional or global scales in terms of spatial and temporal variation analysis of vegetation productivity. GOSIF GPP is often used as baseline data to verify the simulation capability of different light use efficiency (LUE) models in assessing the effects of drought on vegetation productivity. In ecosystem carbon cycle and climate response studies, GOSIF GPP is used to quantify the carbon uptake capacity of vegetation in different climatic zones.

Therefore, using the GOSIF GPP dataset with high accuracy and wide availability helps to clarify the impact of triple La Niña events on total forest primary productivity in China from 2020 to 2022. In order to improve the computational efficiency while still maintaining the key spatial pattern information, it is processed to a spatial resolution of 0.5°. GOSIF GPP data available: https://globalecology.unh.edu/data/GOSIF-GPP.

# 2.3 Land Cover Data

MODIS MCD12Q1 land cover data is used in this study. It has long time series and multiple land cover types. It is one of the most widely used land cover data in the world. It is obtained by supervised classification of reflectance data from MODIS satellites Terra and Aqua, and then further refinement of specific categories through post-processing and ancillary information. It provides a global distribution of land cover types by year with a resolution of 500 meters. This study selected land cover data for 2020 and processed it to the same spatial resolution of 0.5° as the GOSIF GPP dataset. MODIS MCD12Q1 land cover data available: https://modis.gsfc.nasa.gov/data/dataprod/mod12.php.

#### 2.4 Climate Factor Datas

ERA5-Land precipitation, air temperature and soil moisture at root zone (SMroot) data were used in this study. ERA5-Land is a reanalysis dataset that provides a consistent view of the evolution of land variables over decades at a higher resolution than ERA5. ERA5-Land is generated by replaying the ECMWF ERA5 climate reanalysis portion of the land. The spatial resolution of the data is 0.1 degrees, with precipitation and temperature data covering January 1950 to the present, and soil moisture data covering January 1981 to the present, with monthly temporal resolution. During data processing, all three climate data were resampled to a spatial resolution of 0.5°.

CRUJRA v2.4 dataset is a land-surface gridded time series data set developed by the Climate Research Unit (CRU) of the University of East Anglia (UEA) with a spatial resolution of 0.5° and a temporal resolution of 6 hours covering the period January 1901 to December 2022. The dataset is re-gridded based on Japan Reanalysis Data (JRA) from the Japan Meteorological Agency (JMA) and contains climate variables. Although this dataset does not directly provide Vapor Pressure Deficit (VPD) data, it can be calculated using the near-surface specific humidity, surface pressure and air temperature data it contains.

ERA5-Land data available: Muñoz Sabater, J. (2019): ERA5-Land monthly averaged data from 1950 to present. Copernicus Climate Change Service (C3S) Climate Data Store (CDS). DOI: 10.24381/cds.68d2bb30 (Accessed on DD-MMM-YYYY).

CRU JRA data available: University of East Anglia Climatic Research Unit; Harris, I.C. (2023): CRU JRA v2.4: A forcings dataset of gridded land surface blend of Climatic Research Unit (CRU) and Japanese reanalysis (JRA) data; Jan.1901 - Dec.2022.. NERC EDS Centre for Environmental Data Analysis, date of citation. https://catalogue.ceda.ac.uk/uuid/aed8e269513f446fb1 b5d2512bb387ad.

#### 3. Methodology

# 3.1 Detrending Method

Elevated CO<sub>2</sub> concentrations in the atmosphere enhance photosynthesis in plants, a phenomenon known as the CO<sub>2</sub> fertilization effect. Since CO<sub>2</sub> is a key substrate for photosynthesis, increasing its concentration can improve the photosynthetic efficiency of C3 plants, especially under conditions of sufficient nutrients and water. Therefore, when analysing GPP, it is important to consider the effect of CO<sub>2</sub> fertilization on long-term trends, and direct analysis of raw data may lead to seasonal and interannual variability being masked. Therefore, in calculating the annual total GPP, detrend processing is performed to eliminate the influence of long-term trends and make the influence of interannual variations and climatic factors clearer:

$$GPP_{detrended(t)} = GPP_{observed(t)} - (a + b \times t),$$
 (1)

where GPP<sub>observed(t)</sub> is the original GPP observation at year t, a is the intercept term, b is the slope of the linear trend, and t is the time variable. First, linear regression fitting is performed on the annual total GPP time series from 2015 to 2022. The fitted linear trend term is then subtracted from the original series. Finally, the detrended GPP sequence is obtained. This method can effectively remove long-term linear trends from the data and retain interannual fluctuations.

STL (Seasonal-Trend decomposition using Loess) is used to analyze seasonal spatial anomaly and monthly anomaly in key areas. This hierarchical processing strategy can not only keep the simplicity of interannual analysis, but also effectively extract seasonal cycle characteristics of monthly scale data, thus revealing the spatial variation of GPP at different time scales more accurately.

STL is a robust method for decomposing time series, in which Loess is a method for estimating nonlinear relationships. STL can decompose a time series into three main components: trends, seasonal terms, and residuals (Cleveland et al., 1990). Given a y<sub>t</sub> of time series data, STL breaks it down into:

$$y_t = T_t + S_t + R_t , \qquad (2)$$

where  $T_t = Trend$ ,  $S_t = Seasonal$ ,  $R_t = Residual$ . STL uses Loess to extract smoothed estimates of the three components, fulfilling the need to remove the seasonal trend of GPP.

# 3.2 Abnormal Calculation

To quantify how abnormal a period is relative to historical normals, calculate the deviation of actual values (e.g. GPP, temperature, precipitation, etc.) from average conditions for a period using the following formula:

$$A(t) = X(t) - \overline{X}, \qquad (3)$$

where X(t) is the actual value at point t (e.g., a year, month, or day).  $\overline{X}$  is the state average, usually taking the mean of a fixed time period as the benchmark. A(t) is the deviation of the actual value at time t from the reference value, with positive values indicating higher than normal and negative values indicating lower than normal. Different scenarios apply different time periods to calculate annual anomalies, monthly anomalies, seasonal anomalies, etc.  $\overline{X}$  is calculated as follows:

$$\overline{X} = \frac{1}{n} \sum_{i=1}^{n} X_i , \qquad (4)$$

where n is the length of the time series.  $X_{i}$  is the actual value for year i.  $\sum_{i=1}^{n} X_i$  is the sum of actual values over n years.  $\frac{1}{n}$  is the normalization factor for averaging, dividing the sum by the number of years to get the average.

# 3.3 Z-Score Standardized

To eliminate dimensional effects and allow cross-variable, crossregional comparisons, Z-Score is used to normalize regional GPP and climate data to anomalies:

$$A_{std}(t) = \frac{X(t) - \overline{X}}{\tau}, \qquad (5)$$

$$\begin{aligned} A_{std}(t) &= \frac{X(t) - \overline{X}}{\sigma}, \\ \sigma &= \sqrt{\frac{1}{n} \sum_{i=1}^{n} (X_i - \overline{X})^2}, \end{aligned} \tag{5}$$

where X(t) and  $\overline{X}$  are explained.  $\sum_{i=1}^{n} (X_i - \overline{X})^2$  is the sum of the squares of the differences between the actual values and the mean values in n years, and the variance can be obtained by combining the normalization factor  $\frac{1}{n}$ . After square extraction, it is the standard deviation  $\sigma$  of the reference time period. Completes the requirement to show the absolute magnitude of the observed deviation from the mean.

### 3.4 SHAP Analysis

The SHAP model can analyze the contribution and influence of features to the output of the model (Mosca et al., 2022). For model f and input sample x, the Shapley value of feature  $\emptyset_i$ calculated as follows:

$$\emptyset_{i}(f,x) = \sum_{S \subseteq F} \frac{|S|(|F|-|S|-1)!}{|F|!} [f(S \cup \{i\}) - f(S)], \quad (7)$$

where F is the set of all features (total |F| features), S is a subset that does not contain feature i (i.e.,  $S \subseteq F\{i\}$ ), and f(S) is the predicted value of the model when using only a subset of features S, and  $\frac{|S|(|F|-|S|-1)!}{|F|!}$  is the weight (taking into account all possible order of feature combinations). S is calculated by marginalizing other features).

### 4. Results

#### 4.1 Annual GPP Total Anomaly and Climate Zoning Contribution

In analyzing GPP, the effect of CO<sub>2</sub> fertilization on long-term trends must be considered, so detrend treatment is performed in calculating annual total GPP to eliminate the influence of longterm trends and make the influence of interannual variation and climatic factors clearer. According to Figure 3, the Detrended GPP data of China forests from 2015 to 2022 show certain interannual fluctuations, but the overall data remain relatively stable and are within the interval. The average value of these eight years is 1785.44 Tg C year<sup>-1</sup>, the standard deviation is 19.53Tg C year<sup>-1</sup>, the data dispersion is low, and the interannual variation is limited. Specifically, Detrended GPP fluctuated between  $1763.68 \text{ Tg C year}^{-1}$  and  $1823.06 \text{ Tg C year}^{-1}$ , reaching a peak in 2017 (1823.06 Tg C year<sup>-1</sup>), which was about 2.1% higher than the average, and falling to a minimum in 2020 (1763.68 Tg C year<sup>-1</sup>), which was about 1.2% lower than the average. For the remaining years, fluctuations were smaller, ranging within  $\pm 1\sigma$  of the mean.

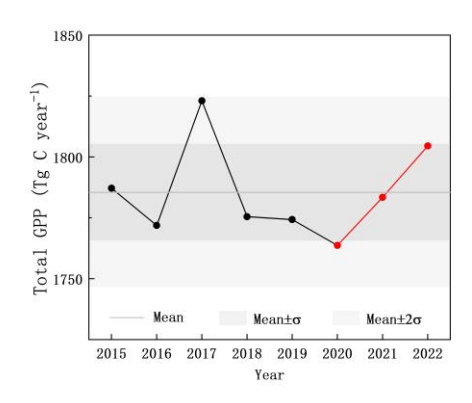


Figure 3. Interannual variation of forest Detrended GPP in China (2015-2022). Broken line is actual value. Purple-red part is triple La Niña event occurrence period. Dark gray solid line is multi-year average value. Light gray and lighter gray areas represent  $\pm 1\sigma$  and  $\pm 2\sigma$  standard deviation range respectively.

Taking into account the strong El Niño event from May 2014 to May 2016 and the impact of high temperature and drought in 2019, the study selected 2017-2018 as the reference period for follow-up analysis.

During the triple La Niña event from 2020 to 2022, the average annual Detrended GPP was 1783.89 Tg C year<sup>-1</sup>, down 15.38 Tg C year<sup>-1</sup> from the baseline period (1799.27 Tg C year<sup>-1</sup>). Among them, there is a 0.6% decrease from 2019 to 2020 (1774.29 Tg C year<sup>-1</sup>→1763.68 Tg C year<sup>-1</sup>). The 2020 value is not only the lowest point during the triple La Niña event, but also the lowest recorded in the entire 2015-2022 observation cycle. Entering 2021, it showed a strong recovery trend, with Detrended GPP jumping to 1783.44 Tg C year<sup>-1</sup>, an increase of about 1.1% compared with 2020. The value jumped to 1804.54 Tg C year<sup>-1</sup> in 2022, up about 1.2% from the previous year and exceeding the eight-year average by about 1.1%.

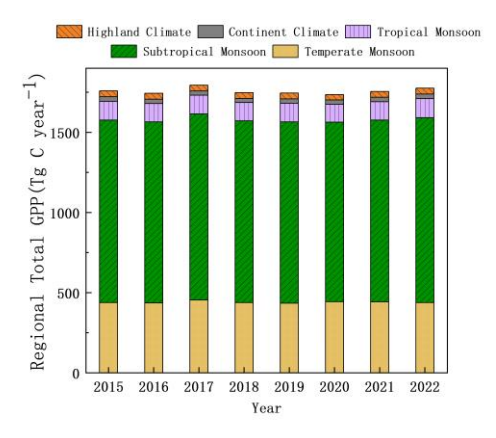


Figure 4. Annual variation of Detrended GPP in five forest climatic regions.

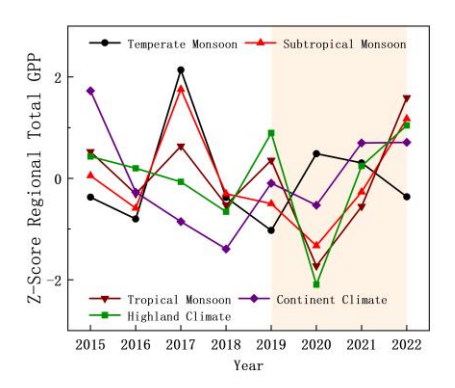


Figure 5. Five forest climatic regions Detrended GPP Z-Score comparison.

Based on this, the response of forest ecosystem in China to triple La Niña event presents phased characteristics: GPP decreases in the early stage of the event (2020), showing short-term inhibition effect; but with the duration of the event (2021-2022), GPP slowly rises, showing certain adaptability and long-term recovery potential of the ecosystem.

The fluctuation characteristics of forest annual total GPP in China are formed by the superposition of forest area responses to different climates. Figure 4 shows that there are significant spatial differences in the contribution of different climatic regions to the change of total Detrended GPP in China forests. Among them, subtropical monsoon climate forest area contributed the most, with an average of 1137.75 Tg C year<sup>-1</sup> in the study period, accounting for 63.7%, becoming the dominant area. The temperate monsoon climate forest area is the second, with an average of 440.69 Tg C year<sup>-1</sup> and a contribution rate of

24.7%. In contrast, the contribution of tropical monsoon climate forest areas is relatively limited, accounting for only 6.5%, and the contribution of other two climate types forest areas is relatively weak. This distribution pattern clearly reflects the significant regional heterogeneity of forest GPP changes in China.

In view of the significant magnitude difference in the contribution of five climatic forest regions to GPP, Z-Score normalization method was used to normalize the data of each climatic region to eliminate the dimensional effect, so as to compare the relative variation trend of GPP fluctuation in different climatic regions more clearly. This normalization helps to reveal the synchronicity or diversity of GPP changes in different climatic regions.

The GPP normalized by five climatic zones showed different fluctuation characteristics during the period. Temperate monsoon climate forest area fluctuates most violently, reaching peak in 2017 (2.14 $\sigma$ ), falling to trough in 2019 (-1.03 $\sigma$ ); the overall fluctuation of subtropical monsoon climate forest area is relatively gentle, but significant negative anomaly will appear in 2020.(-1.33 $\sigma$ ), rising to positive again in 2022 (1.18 $\sigma$ ); tropical monsoon climate forest area has the largest fluctuation amplitude, with an extreme low value (-1.73 $\sigma$ ) in 2020 and a rebound to the highest value (1.59 $\sigma$ ) in 2022; temperate continental climate forest area has a significantly higher value (1.73 $\sigma$ ) in 2015, and fluctuates in negative range in subsequent years; plateau mountain climate forest area has an abnormal low value (-2.09 $\sigma$ ) in 2020, and other years fluctuate slightly near zero value.

On the whole, the GPP fluctuation of each climate zone is synchronous. For example, each climate zone shows obvious negative anomaly in 2020, among which the synchronous decline of subtropical monsoon climate forest area, tropical monsoon climate forest area and plateau mountain climate forest area is especially prominent. While in 2022, except temperate monsoon climate forest area, the other four climate zones show synchronous recovery trend, especially the rebound amplitude of tropical monsoon climate forest area and subtropical monsoon climate forest area is the most significant. At the same time, the GPP fluctuation of each climate zone shows obvious regional differences. During the triple La Niña event, except temperate monsoon climate forest area, GPP in the other four climatic regions showed a trend of "decreasing first and then increasing," which directly affected the interannual variation pattern of total GPP in China. The temperate monsoon climate forest area region showed a different response pattern from other climate regions, and its GPP showed an anti-phase change characteristic of "first increasing and then decreasing."

#### 4.2 Analysis of Seasonal Spatial Anomalies

In order to highlight seasonal characteristics, differential data processing methods are used in spatial analysis: Detrend is directly used for annual GPP analysis to eliminate the influence of long-term trend; STL decomposition method is used in seasonal spatial anomaly analysis in this section and monthly scale anomaly analysis in the next section. This hierarchical processing strategy can not only keep the simplicity of interannual analysis, but also effectively extract seasonal cycle characteristics of monthly scale data, thus revealing the spatial variation of GPP at different time scales more accurately.

Firstly, the forest GPP anomalies in China showed significant seasonal differences, with the fluctuation amplitude in spring and summer being significantly greater than that in autumn and winter (Figure 6). In 2020, the average anomalies in spring and

summer are -4.16 gC m $^{-2}$  mon $^{-1}$  and 2.65 gC m $^{-2}$  mon $^{-1}$  respectively, while the average anomalies in autumn and winter are smaller (-0.82 gC m $^{-2}$  mon $^{-1}$  and-0.44 gC m $^{-2}$  mon $^{-1}$ ). Similar trends continued in 2021–2022. Notably, the anomaly range in 2022 autumn expands to -29.24 gC m $^{-2}$  mon $^{-1}$  to 26.60 gC m $^{-2}$  mon $^{-1}$ .

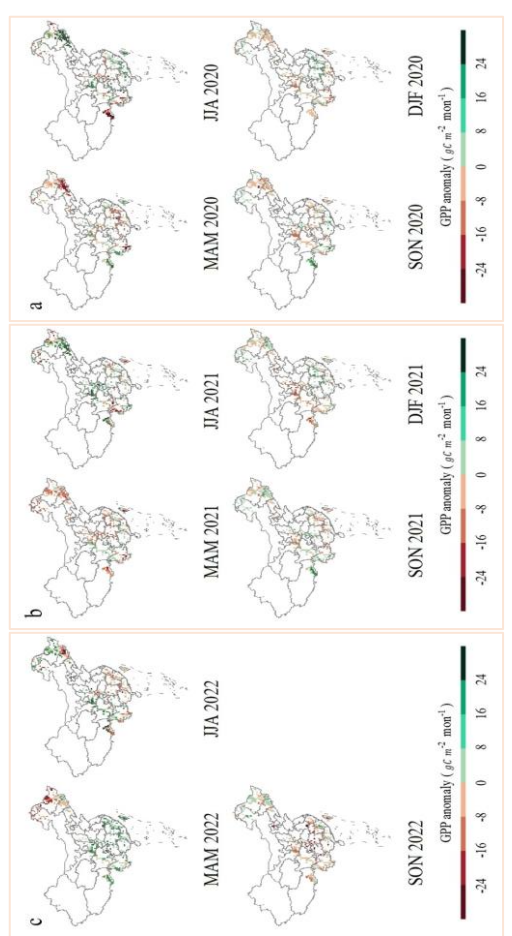


Figure 6. Spatial anomaly distribution of forest GPP in China from spring 2020 to autumn 2022. (a) 2020;(b) 2021;(c) 2022. Green indicates an abnormal increase in GPP and red indicates an abnormal decrease (relative to the 2017-2018 average for the same period).

anomalies showed significant differentiation. In the spring of 2020, 68.1% of the regions in China showed negative GPP anomalies, especially in the three eastern provinces and the south; while in summer, there was obvious spatial pattern transformation, and the three eastern provinces and the southeast coastal areas turned to positive anomalies. This feature continues in 2021. In spring, 70.8% of the areas (mainly distributed in the three eastern provinces and the central and eastern parts) present negative anomalies, but in summer, the southern parts of the three eastern provinces, the southeast of Xizang and central parts (Shanxi and Hubei) turn into positive anomalies. In 2022, the spatial pattern is quite different from that of the previous two years: 65.3% of the regions present positive anomalies in spring, and significant spatial differentiation is formed in the south and northeast; in summer, the southeast changes from positive anomalies to negative anomalies, while the north of Inner Mongolia and the north of the three eastern provinces show opposite changes. This spatial differentiation is closely related to the fact that China spans multiple climatic zones.

# 4.3 Analysis of Key Areas

In view of the significant spatial heterogeneity of forest GPP anomalies in China, and the contribution of forests in temperate monsoon climate zone and subtropical monsoon climate zone to the total GPP of China is more than 88%, this study focuses on these two key regions.

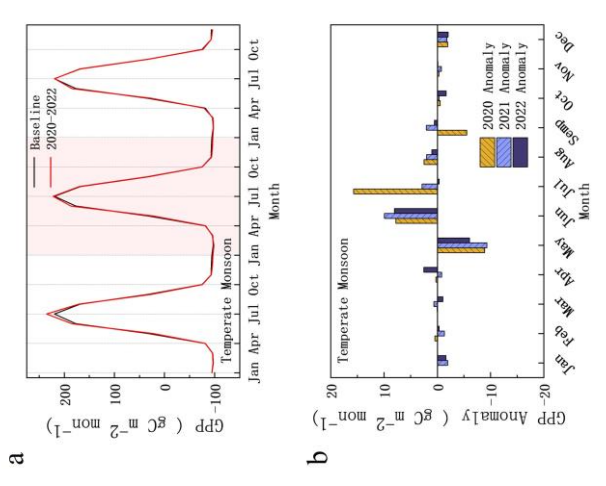


Figure 7. Characteristics of GPP monthly variation in temperate monsoon climate forest area of China (base period vs. 2020-2022).

(a)Comparison of monthly GPP averages for the baseline period and 2020-2022;(b) Monthly relative outliers for GPP 2020-2022.

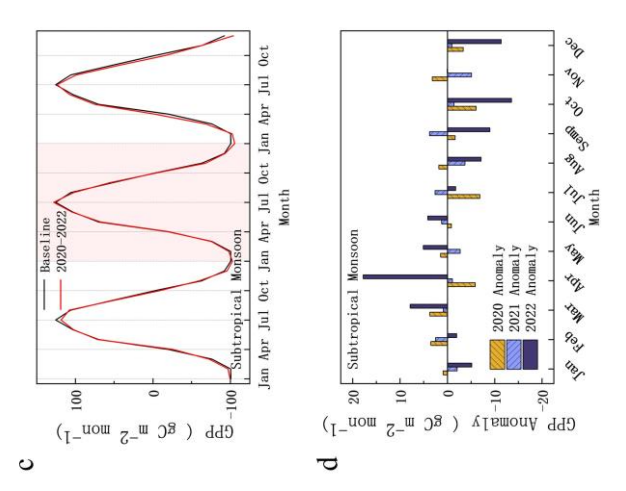


Figure 8. Characteristics of GPP monthly variation in subtropical monsoon climate forest area of China (base period vs. 2020-2022).

(c)Comparison of monthly GPP averages for the baseline period and 2020-2022;(d) Monthly relative outliers for GPP 2020-2022.

Between 2020 and 2022, the GPP in temperate monsoon climate forest area exceeded the baseline level observed in 2019. However, there has been a consistent decrease in GPP annually during this period, a trend likely influenced by the interannual variability of climate factors.

According to Figure 9, the precipitation in this area will increase by 0.25 mm and 0.49 mm on average in 2020 and 2021 respectively, while it will decrease slightly by 0.03 mm in 2022. This change of precipitation pattern reflects the interannual difference of regional water circulation process. The temperature continues to be high in the same period, but the increase decreases year by year, and increases by 0.83 K, 0.37 K and 0.10 K respectively in three years, indicating that the climate warming trend is still continuing but the intensity has slowed down. SMroot content increased steadily, with an increase of 0.003  $m^3m^{-3}$ , 0.021  $m^3m^{-3}$  and 0.015  $m^3m^{-3}$  respectively, while saturated vapor pressure difference (VPD) increased first and then decreased, with a significant increase of 62.90 Kpa in 2020 and a decrease of 41.21 Kpa and 32.89 Kpa respectively from 2021 to 2022. This change pattern reflected the phased mitigation of atmospheric drought.

From the perspective of seasonal dynamics (Figure 7(a)), GPP in this region reaches its peak in July every year, but the peak intensity decreases year by year. GPP in July 2020 is 15.72 gC m<sup>-2</sup> higher than that in the baseline period, and the amplitude of high in 2021 decreases to 2.85 gC m<sup>-2</sup>, while it turns to 0.33 gC m<sup>-2</sup> lower in 2022. According to Figure 7 (b), anomaly analysis shows that GPP fluctuation is mainly concentrated in May-July, showing obvious regular changes: GPP is continuously low in May accompanied by significant low temperature (0.49 k, 1.56 k and 1.42 k lower in three years respectively), while it turns to positive anomaly in June and its amplitude is equivalent to that of negative anomaly in May. This change is closely related to temperature recovery (Figure 11), especially the temperature in June from 2021 to 2022 is higher than that of baseline period 0.18 k and 0.24 k.

In the first year of La Niña event (2020), GPP in subtropical monsoon climate forest area was suppressed, but it showed strong recovery ability in the following two years. This dynamic change is closely related to the evolution of regional climatic factors. The data show (Figure 10) that precipitation increases first and then decreases, increasing by 0.43 mm in 2020, weakening to 0.06 mm in 2021 and decreasing by 0.41 mm in 2022. Temperature fluctuated and increased by 0.005 K, 0.35 K and 0.096 K in three years, respectively, and the significant warming in 2021 may play a key role in vegetation restoration. It is worth noting that SMroot content continues to decrease, decreasing by 0.005  $\rm m^3 m^{-3}$ , 0.005  $\rm m^3 m^{-3}$  and 0.008  $\rm m^3 m^{-3}$  respectively in three years, while VPD shows an accelerated upward trend, increasing from 6.61 Kpa in 2020 to 48.00 Kpa in 2022, indicating that atmospheric drought continues to intensify.

Figure 8 (c) shows that GPP dynamics in subtropical monsoon climate forest area show different characteristics from those in temperate regions. Although GPP also peaks in July in this region, the interannual variation in peak intensity is opposite to that in temperate regions: the lowest in 2020 and the highest in 2021. Outlier distribution characteristics are more complex. Temporally, the outliers are not concentrated in a specific month, but scattered throughout the year. The interannual difference is significant. In 2020, the positive and negative abnormal months are half, but the negative abnormal intensity is greater; in 2021, the negative abnormal months are dominant (7 months), but the overall abnormal degree is weaker than that in 2020. Of particular concern is the anomaly pattern in 2022: significant negative anomalies (8.96 gC m<sup>-2</sup>, 13.55 gC m<sup>-2</sup>, 11.37 gC m<sup>-2</sup> respectively) in autumn (September-October) and winter (December), while strong positive anomalies appear in spring

(March-June), with an anomaly increase of  $17.80~{\rm gC~m^{-2}}$  in April.

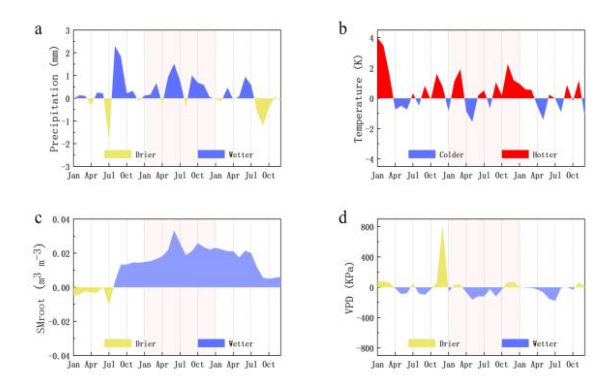


Figure 9. Climate factor anomalies in temperate monsoon climate forest area of China (base period vs. 2020-2022). (a)Monthly relative anomaly of precipitation from 2020 to 2022;(b) Monthly relative anomaly of temperature from 2020 to 2022;(c) Monthly relative anomaly of SMroot from 2020 to 2022;(d) Monthly relative anomaly of VPD from 2020 to 2022.

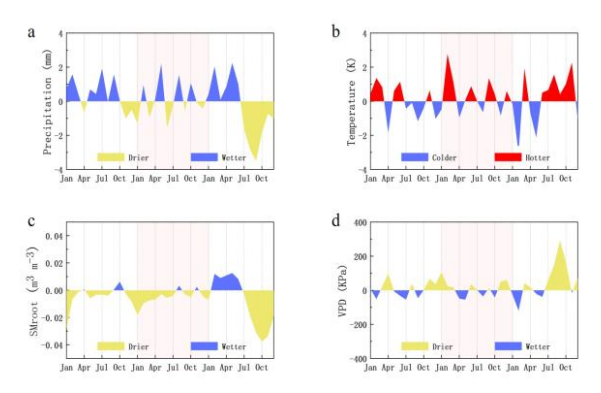


Figure 10. Climate factor anomalies in subtropical monsoon climate forest area of China (base period vs. 2020-2022).
(a)Monthly relative anomaly of precipitation from 2020 to 2022;(b) Monthly relative anomaly of temperature from 2020 to 2022;(c) Monthly relative anomaly of SMroot from 2020 to 2022;(d) Monthly relative anomaly of VPD from 2020 to 2022.

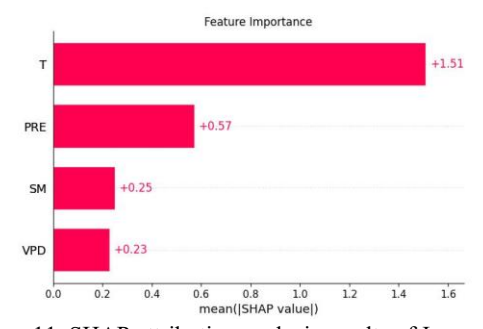


Figure 11. SHAP attribution analysis results of June reverse May negative anomaly in temperate monsoon climate forest area of China.

#### 5. Discussion

# 5.1 GPP Spatio-temporal Changes and Zoning Comprehensive Discussion

This study reveals the complex response mechanism of forest GPP in China to climate events through multi-time scale analysis.

In terms of time scale, different data processing strategies were adopted: interannual analysis used detrend processing to eliminate long-term trend effects, while seasonal and monthly analysis used STL decomposition method to extract seasonal cycle characteristics. This method effectively captures the variation law of GPP anomalies on different time scales.

The data show that the national average annual GPP is  $1785.44 \pm 19.53$  Tg C year<sup>-1</sup>, which drops to 1783.89 Tg C year<sup>-1</sup> during La Niña event (2020-2022), 0.86% lower than 1799.27 Tg C year<sup>-1</sup> in base period (2017-2018). This decrease is mainly due to a significant inhibitory effect at the beginning of the event (2020), when GPP fell to 1763.68 Tg C year<sup>-1</sup>, the lowest value in the study period. However, the GPP recovered to 1783.44 and 1804.54 Tg C year<sup>-1</sup> in the following two years. This "initial inhibition-gradual recovery" change pattern not only reflects the short-term impact of extreme climate events, but also reveals that China's forest ecosystem has certain adaptive capacity and long-term recovery potential.

The results showed that GPP anomalies in China forest showed significant seasonal and spatial differentiation characteristics. On the seasonal scale, the fluctuation amplitude in spring and summer is obviously larger than that in autumn and winter. This pattern is closely related to seasonal variations in vegetation phenology and climatic conditions. Greening of vegetation in spring and vigorous photosynthesis in summer lead to enhanced GPP, and extreme weather events trigger violent fluctuations in carbon emissions (Deng et al., 2021). In contrast, vegetation activity weakened in autumn and winter, and GPP changed relatively gently. From the perspective of vegetation phenology, spring is the key period at the beginning of the growing season, and phenological processes such as budding and leafing of deciduous trees and restoration of photosynthetic activity of evergreen trees are very sensitive to temperature and moisture(Lapointe, 2001). Summer is the peak season for vegetation growth (Chen et al., 2000). In autumn of 2022, the anomaly was significantly strengthened and its range expanded, which reflected the cumulative effect of ecosystem carbon cycle under the background of long-term climate change (Frank et al., 2015). In terms of spatial pattern, GPP anomalies show obvious regional differentiation. 2020-2021 In 2020, the three eastern provinces and the southern region generally showed negative anomalies (68.1%-70.8% area) in spring and turned to positive anomalies in summer, while the spatial pattern reversed in 2022, with positive anomalies in 65.3% area in spring and positive anomalies in southeast in summer. This spatial differentiation is closely related to the geographical characteristics of China spanning multiple climatic zones, especially the transition zone between temperate and subtropical monsoon climatic zones.

The response of different climatic regions to La Niña events is different. Subtropical monsoon climate region is the largest carbon sink contributing region (annual average GPP 1137.75 Tg C year  $^{-1}$ , accounting for 63.7% of the total), and its GPP appears significant negative anomaly (-1.33 $\sigma$ ) in 2020, but quickly returns to positive anomaly (+1.18 $\sigma$ ) in 2022. Temperate monsoon climate region (annual average GPP 440.69 Tg C year  $^{-1}$ , accounting for 24.7%) shows unique anti-phase response characteristics, relatively high in 2020 and low in 2022. The GPP fluctuates most violently in tropical monsoon climate region, with the anomaly reaching -1.73 $\sigma$  in 2020 and bouncing back to +1.59 $\sigma$  in 2022.

The formation mechanism of this regional difference is mainly related to the following factors: First, the prominent response of temperate and subtropical monsoon climate zones is closely related to their special ecological and geographical characteristics. These two regions not only have the largest forest resources in China, but also are close to the ocean, so that the ocean-atmosphere coupling anomaly caused by La Niña event can affect these regions first and most strongly through atmospheric circulation (Wu et al., 2010). This unique geographic location makes it a critical transition zone linking ocean climate anomalies with terrestrial ecosystem responses. Secondly, different vegetation composition (Lloret et al., 2012) (e.g., evergreen broad-leaved forest vs. deciduous forest) and environmental adaptation strategies (e.g., differences in water and heat use efficiency) further shape their response characteristics. Finally, specific combinations of climatic factors at regional scales result in differences in observed GPP spatial and temporal patterns by regulating plant phenology and physiological processes.

### 5.2 Regional Response Gap Analysis Discussion

The differential responses of temperate and subtropical monsoon forest regions to La Niña events revealed in this study are essentially due to the latitudinal differential regulation mechanism of the climate events on the East Asian monsoon system.

In the temperate monsoon climate forest area, La Niña mainly affects through enhanced winter monsoon circulation and meridional temperature gradient change: strong cold air southward leads to significant low temperature in spring of 2020. This hydrothermal allocation explains the observed increase in SMroot and VPD. In contrast, the subtropical monsoon climate forest area is more directly regulated by tropical SST anomalies: the continuous strengthening of the western Pacific subtropical high leads to the increase and decrease of precipitation (Yang et al., 2022), accompanied by the continuous increase of VPD and the drought of soil. This difference reflects the spatial-scale characteristics of the impact of the La Niña event, the temperate zone is mainly regulated by atmospheric teleconnection at middle and high latitudes, while the subtropical zone directly responds to the tropical air-sea coupling process (Zi et al., 2022). This fundamental driving difference is the reason for the two climate zones. The underlying reasons for the different GPP response patterns.

Temperature, precipitation, SMroot and VPD are four key climatic factors regulating vegetation photosynthesis. Temperature regulates photosynthesis by directly affecting enzymatic reaction rate and membrane stability, and its effect shows a single-peak curve: in the appropriate temperature range, heating can increase Rubisco enzyme activity, but exceeding the threshold will lead to negative effects (Salvucci and Crafts -Brandner, 2004). Precipitation and soil water content determine the water status of plants together. The decrease of soil water content will cause the decrease of xylem water potential, induce stomatal closure through ABA signal pathway, and weaken the activity of electron transport chain (Liu et al., 2022). VPD reflects the degree of atmospheric drought, and its increase will aggravate plant transpiration and water loss (López et al., 2021). When the atmosphere is too dry, it will not only promote stomata closure, but also directly damage photosynthetic membrane system (Arve et al., 2011). There are complex interactions among these factors, such as high temperature with high VPD will aggravate water stress, and moderate temperature may promote photosynthesis when water is sufficient (Will et al., 2013).

The interannual variation of GPP in temperate monsoon climate forest area reflects the complex regulation mechanism of climate

factors on photosynthesis. The study shows that although annual precipitation fluctuates little, SMroot continues to rise. A special water supply pattern was formed: on the one hand, it improved the water availability of vegetation, on the other hand, excessive soil water had negative effects on photosynthesis by inhibiting root respiration and inducing abnormal stomatal opening. At the same time, moderate temperature increase can increase Rubisco enzyme activity. With the regulation of VPD increasing first and then decreasing, the synergistic effect of these factors finally showed the trend of GPP decreasing year by year, indicating that soil moisture excess had become a more critical photosynthetic limiting factor than temperature change in this region. It should be noted that the seasonal dynamics of GPP showed a significant "early stage determines late stage" characteristic: persistent low temperature in May could cause persistent low leaf area index at key growth stages by delaying phenological process (Bhattacharya, 2022). The cumulative effect of this early stress explained why the peak intensity of GPP decreased year by year in July.

The response of GPP to La Niña events in subtropical monsoon climate forest area presents a typical three-stage dynamic characteristic of "suppression-adaptation-recovery," which is closely related to the coordinated change of regional water and heat conditions. At the beginning of the event, although precipitation increased, a special hydrothermal configuration was formed with a slight increase in temperature and an increase in VPD: the evapotranspiration effect of increased warming caused the new precipitation to be rapidly consumed, while the SMroot still decreased. This seemingly contradictory moisture condition induced partial closure of stomata through ABA signaling pathway, which directly restricted the intercellular diffusion of CO<sub>2</sub>, resulting in significant inhibition of GPP. With the continuous development of the event, the climate stress showed an aggravating trend: precipitation increased and decreased, temperature continued to increase, VPD increased, soil moisture decreased, forming a typical high temperature and drought combined stress. Under this environment, vegetation can initiate multi-level adaptation strategies: adjusting VPD response threshold of stomatal opening and closing in short-term response level (Zi et al., 2022); enhancing osmotic regulation ability and photosynthetic apparatus stability in medium-and long-term adaptation level (Hsiao et al., 1976). These physiological adjustments enable the ecosystem to maintain its basic carbon sink function under continuous stress, showing the unique environmental adaptability of subtropical evergreen forests.

# 6. Conclusions

This study elucidates the intricate response mechanism of the forest ecosystem in China to the La Niña event and yields the following crucial findings. Initially, in terms of temporal dynamics, the gross primary productivity (GPP) of China forest exhibits distinct features of "initial suppression-gradual recovery" during the La Niña event (2020-2022). The national average annual GPP declined from 1799.27 Tg C year<sup>-1</sup> in the reference period (2017-2018) to 1783.89 Tg C year<sup>-1</sup> (a decrease of 0.86%) during this event. Specifically, it reached its lowest point of 1763.68 Tg C year<sup>-1</sup> in 202 but steadily rose to 1804.54 Tg C year<sup>-1</sup> in the subsequent two years. This recovery trend underscores the robust climate resilience of forest ecosystems in China, albeit with notable variations across regions and seasons.

Secondly, in the spatial pattern, the study found obvious regional differentiation characteristics. Subtropical monsoon climate region is the main contributor (63.7%), and its GPP shows a

typical "V" rebound, while temperate monsoon climate region (24.7%) shows a unique anti-phase response. This difference is due to the latitudinal difference regulation of La Niña event on East Asian monsoon system: temperate zone is mainly affected by the adjustment of mid-high latitude atmospheric circulation, subtropical zone directly responds to tropical sea surface temperature (SST) anomaly and experiences continuous aridity process. From the physiological mechanism angle, the regulation function of key climatic factors was clarified. The decline of GPP in temperate zone was mainly limited by soil moisture at root zone (SMroot) and delayed spring phenology, while the recovery ability in subtropical zone depended on physiological adaptation at multiple levels. These findings provide a new physiological basis for understanding climate adaptation thresholds in forest ecosystems.

Finally, the study reveals the important regulation law of seasonal scale. The fluctuation amplitude of GPP in spring and summer was significantly larger than that in autumn and winter, and the temperate zone showed the characteristic of "early stage determines late stage", while the subtropical zone formed the pattern of "spring and autumn compensation". These seasonal dynamics reflect the differences in adaptive strategies of different functional vegetation types and are of great value to improve phenological parameterization in ecosystem models.

Through multi-scale analysis, this study not only clarified the response mechanism of forests in China to climate events, but also provided scientific basis for predicting the evolution of carbon sink function under the background of global change. Future studies need to combine long-term observations and multi-omics approaches to further elucidate the genetic basis of vegetation adaptation and its interaction with climate variability.

# 7. Acknowledgements

This work was supported by the National Natural Science Foundation of China (Grant No. 42201381) and the Program of Beijing Scholar.

#### References

Arve, L., Torre, S., Olsen, J., and Tanino, K., 2011: Stomatal responses to drought stress and air humidity, in: Abiotic stress in plants-Mechanisms and adaptations, IntechOpen.

Bastos, A., Gouveia, C. M., Trigo, R. M., and Running, S. W., 2014: Analysing the spatio-temporal impacts of the 2003 and 2010 extreme heatwaves on plant productivity in Europe. *Biogeosciences*, 11, 3421-3435, 10.5194/bg-11-3421-2014.

Best, J. and Darby, S. E., 2020: The pace of human-induced change in large rivers: Stresses, resilience, and vulnerability to extreme events. *One Earth*, 2, 510-514.

Bhattacharya, A., 2022: Effect of low-temperature stress on germination, growth, and phenology of plants: A review. *Springer Singapore eBooks*, 1-106.

Chen, X., Tan, Z., Schwartz, M. D., and Xu, C., 2000: Determining the growing season of land vegetation on the basis of plant phenology and satellite data in Northern China. *International Journal of Biometeorology*, 44, 97-101.

Cleveland, R. B., Cleveland, W. S., McRae, J. E., and Terpenning, I., 1990: STL: A seasonal-trend decomposition. *Journal of official statistics*, 6, 3-73.

- Deng, Y., Wang, X., Wang, K., Ciais, P., Tang, S., Jin, L., Li, L., and Piao, S., 2021: Responses of vegetation greenness and carbon cycle to extreme droughts in China. *Agricultural and Forest Meteorology*, 298, 108307.
- Frank, D., Reichstein, M., Bahn, M., Thonicke, K., Frank, D., Mahecha, M. D., Smith, P., Van der Velde, M., and Vicca, S., 2015: Effects of climate extremes on the terrestrial carbon cycle: concepts, processes and potential future impacts. *Global Change Biology*, 21, 2861-2880.
- Hsiao, T. C., Acevedo, E., Fereres, E., and Henderson, D., 1976: Water stress, growth and osmotic adjustment. *Philosophical Transactions of the Royal Society of London. B, Biological Sciences*, 273, 479-500.
- Lapointe, L., 2001: How phenology influences physiology in deciduous forest spring ephemerals. *Physiologia Plantarum*, 113, 151-157.
- Liu, H., Song, S., Zhang, H., Li, Y., Niu, L., Zhang, J., and Wang, W., 2022: Signaling transduction of ABA, ROS, and Ca2+ in plant stomatal closure in response to drought. *International Journal of Molecular Sciences*, 23, 14824.
- Lloret, F., Escudero, A., Iriondo, J. M., Martínez-Vilalta, J., and Valladares, F., 2012: Extreme climatic events and vegetation: the role of stabilizing processes. *Global Change Biology*, 18, 797-805.
- López, J., Way, D. A., and Sadok, W., 2021: Systemic effects of rising atmospheric vapor pressure deficit on plant physiology and productivity. *Global Change Biology*, 27, 1704-1720.
- Mosca, E., Szigeti, F., Tragianni, S., Gallagher, D., and Groh, G., 2022: SHAP-based explanation methods: a review for NLP interpretability. Proceedings of the 29th international conference on computational linguistics, 4593-4603.
- Salvucci, M. E. and Crafts-Brandner, S. J., 2004: Inhibition of photosynthesis by heat stress: the activation state of Rubisco as a limiting factor in photosynthesis. *Physiologia plantarum*, 120, 179-186.
- Will, R. E., Wilson, S. M., Zou, C. B., and Hennessey, T. C., 2013: Increased vapor pressure deficit due to higher temperature leads to greater transpiration and faster mortality during drought for tree seedlings common to the forest–grassland ecotone. *New Phytologist*, 200, 366-374.
- Wolf, S., Paul-Limoges, E., 2023: Drought and heat reduce forest carbon uptake. *Nat Commun*, 14, 6217, https://doi.org/10.1038/s41467-023-41854-x.
- Wu, B., Li, T., and Zhou, T., 2010: Asymmetry of atmospheric circulation anomalies over the western North Pacific between El Niño and La Niña. *Journal of Climate*, 23, 4807-4822.
- Yang, K., Cai, W., Huang, G., Hu, K., Ng, B., and Wang, G., 2022: Increased variability of the western Pacific subtropical high under greenhouse warming. *Proceedings of the National Academy of Sciences*, 119, e2120335119.
- Zi, Y., Xiao, Z., Yan, H., and Xu, J., 2022: Sub-seasonal east—west oscillation of the western pacific subtropical high in summer and its air—sea coupling process. *Climate Dynamics*, 58, 115-135.